Effect of phosphoric acid purity on the electrochemically active surface area of Pt-based electrodes

Bruna F. Gomes, Martin Prokop, Tomas Bystron, Rameshwori Loukrakpam, Carlos M. S. Lobo, Maximilian Kutter, Timon E. Günther, Michael Fink, Karel Bouzek, Christina Roth

Angaben zur Veröffentlichung / Publication details:

Gomes, Bruna F., Martin Prokop, Tomas Bystron, Rameshwori Loukrakpam, Carlos M. S. Lobo, Maximilian Kutter, Timon E. Günther, Michael Fink, Karel Bouzek, and Christina Roth. 2022. "Effect of phosphoric acid purity on the electrochemically active surface area of Pt-based electrodes." *Journal of Electroanalytical Chemistry* 918: 116450. https://doi.org/10.1016/j.jelechem.2022.116450.

Effect of phosphoric acid purity on the electrochemically active surface area of Pt-based electrodes

Bruna F. Gomes [a,1,*], Martin Prokop [b,1], Tomas Bystron [b,1], Rameshwori Loukrakpam [a], Carlos M.S. Lobo [c], Maximilian Kutter [a], Timon E. Günther [a], Michael Fink [a], Karel Bouzek [b], Christina Roth [a]

[a] Chair of Electrochemical Process Engineering, University of Bayreuth, Universitätsstraße 30, Bayreuth, 95447, Germany, 95447 Bayreuth, Germany
[b] Department of Inorganic Technology, University of Chemistry and Technology Prague, Technicka 5, Prague 6 166 28, Czech Republic
[c] Institute for Technical Chemistry, University of Stuttgart, Pfaffenwaldring 55, 70569 Stuttgart, Germany

ARTICLE INFO

Keywords:
Phosphoric acid
Oxygen reduction reaction
Fuel cells
Phosphorous acid
High temperature pem fuel cell
Phosphoric acid purification

ABSTRACT

In this work, the effect of H_3PO_4 purity on the activity of Pt/C thin film catalysts towards the oxygen reduction reaction (ORR) was investigated. H_3PO_4 is routinely introduced in the electrolyte during rotating disk electrode (RDE) measurements to simulate the existing environment within high-temperature proton exchange membrane fuel cells (HT-PEMFC). Three different purity grades were tested: crystalline (99.99% purity), commercial H_3PO_4 solution (85 wt%), hereafter, designated as non-purified H_3PO_4, and commercial H_3PO_4 solution (85 wt%) purified with H_2O_2. H_3PO_4 and/or its anions are known to strongly adsorb and interact with Pt surfaces. The presence of H_3PO_4 negatively affected the electrochemically active surface area (ECSA) measured by H_{upd} ($ECSA_H$), and by CO stripping ($ECSA_{CO}$), kinetic parameters in the high current density region and the limiting current density (j_{lim}) of ORR. One major finding was that the crystalline and purified H_3PO_4 solutions have similar effects on the Pt/C catalyst activity while the non–purified H_3PO_4 showed a significantly more negative effect on the ECSA as well as on the ORR measurements. This was found to be due to the presence of H_3PO_3 in the non-purified H_3PO_4 solution. Adsorption isotherms of H_3PO_3 were also measured using H_{upd} and CO stripping in order to evaluate its adsorption on the catalyst surface. From these investigations, the purity level of H_3PO_4 was shown to be an important factor in reliable ORR testing.

1. Introduction

Fuel cells (FCs) are gaining significant attention as an alternative technology for converting the chemical energy in H_2 and O_2 bonds into electrical energy with zero CO_2 emissions [1]. Of the existing fuel cell technologies, high temperature proton-exchange membrane fuel cells (HT-PEMFCs) are one of the most promising ones. HT-PEMFCs use a polybenzimidazole (PBI) membrane doped with H_3PO_4 (to ensure proton conductivity) and porous electrodes made from carbon-supported platinum catalysts (Pt/C), which allow the cell to be operated at temperatures ranging from 120 to 200 °C. This enables improved reaction kinetics, increased tolerance to contaminants present in H_2 sources (such as CO and SO_x) and makes heat recovery feasible, thereby reducing the operating costs of the fuel cell [2,3].

Despite the advantages of HT-PEMFCs, some challenges still remain before this technology is applicable at an industrial scale [4]. A substantial part of the encountered issues is related to the lack of long-term stability of the Pt-based catalyst [5,6] and slow kinetics of the electrode reactions due to the poisoning of the catalytic sites with adsorbed H_3PO_4 [7–10]. This results in reduced catalytic activity especially towards O_2 reduction at the cathode side as reported in literature [5,11]. Additionally, H_3PO_4 can be electrochemically reduced by H_2 on the Pt surface to phosphorus species in a lower valence state, such as H_3PO_3, which has been shown to have an even greater poisoning effect on Pt-based electrodes. Indeed, H_3PO_3 competes with both O_2 and H_2 for the Pt active sites, further contributing to the deterioration of the FC's performance [12–14]. It is noteworthy that, while combing through literature, not many published studies specify the purity of H_3PO_4 or even consider it as an important factor [13,15,16]. However, we believe that this factor can significantly affect the rate of O_2 reduction and H_2 oxidation reactions by influencing the availability of the adsorption sites and/or changing kinetic parameters such as the exchange current density and Tafel slope.

* Corresponding author.
E-mail address: bruna.lobo@uni-bayreuth.de (B.F. Gomes).
[1] These authors contributed equally for this publication.

It is worth noting that several works in the literature have already demonstrated how impurities can affect the electrochemical performance in different systems, resulting in inaccurate results. Trotochaud et al. [17] demonstrated that the contamination with Fe ions can significantly alter the performance of Ni-based ORR catalysts and, therefore, the electrolyte and glassware purification are very important steps. Another example is the effect of alumina in the hydrogen evolution reaction using gold-based catalysts. Monteiro et al. [18] reported that the presence of alumina used for polishing the electrode surface can release Al^{3+} ions, which can improve the catalytic performance of gold. A curious fact is that the $Al(OH)_3$ adsorbed on the surface of the electrode is not detectable by gold blank voltammetry. Mayrhofer et al. [19,20] and Tiwari et al. [21] demonstrated that the use of glassware in alkaline medium can also be a source of contamination, since the glass can be dissolved and the impurities can change the electrochemical response dramatically. The majority of these works deal with cationic metal impurities. However, these can be avoided using H_3PO_4 of a high purity grade, which is always stated in the specifications listed by the manufacturer. In our case, the focus was on the presence of reduced phosphorus compounds (with phosphorus oxidation number lower than + 5) that are nearly always present in pure H_3PO_4 due to acid production (usually phosphorus oxidation process). These compounds are not included in the specifications, as they are not considered as impurities by manufacturers. However, the effect of these compounds on the electrochemical behaviour of Pt-based electrodes is, especially in the case of H_3PO_3, tremendous. Therefore, it is important to check all possible forms of contamination to avoid severe reproducibility issues.

The most popular methods currently used to determine the ECSA of Pt-based catalysts are hydrogen underpotential deposition (H_{upd}) and CO stripping [22]. Both methods are similar in that the charge (Q_H and Q_{CO}, respectively) associated with the electro(de)sorption of a (H^+ or CO, respectively) monolayer on the catalyst sites (at a given applied potential) must first be determined. The obtained values are then normalised by the specific charge of the surface area (Q_S) considering an ideal electron transfer processes: a one-electron transfer in the case of H_{upd} (210 μC cm^{-2}) and a two-electron transfer process for CO stripping (390 μC cm^{-2}) [23–25], as shown by Equation (1) [26]. Pure Pt nanoparticle catalysts are expected to show a charge ratio of (Q_{CO} /2 Q_H) ~ 1. However, underestimation of the $ECSA_H$ due to suppression of H_{upd} adsorption is often observed in various experimental conditions [23]. An alternative explanation for this observation is that the Q_H on polycrystalline Pt is underestimated. This is a result of the commonly accepted but unwarranted assumption that the charging current (usually determined in the double layer region of the Pt voltammogram) is independent of the electrode potential, i.e. that it remains constant even when the double layer structure changes in the H_{upd} region. Thus, in certain cases, the charging current can easily be overestimated. This applies even to inert supporting electrolytes such as $HClO_4$ and the situation is likely to be even more complicated in the presence of adsorbing electrolytes such as H_3PO_4. It is recommended that CO stripping be used in conjunction with H_{upd} to avoid underestimating the ECSA, especially since there is yet to be a consensus among the scientific community regarding the best choice of method to determine the ECSA [26].

$$ECSA_{H,CO} = \frac{Q_{H,CO}}{Q_S} \quad (1)$$

In this work, the effect of H_3PO_4 purity on the ORR activity and the ECSA (determined with both CO stripping and H_{upd}) is investigated using the RDE method. To this end, adsorption isotherms for H_3PO_3 on polycrystalline Pt sheets and on Pt/C catalysts were also studied to evaluate its adsorption on the catalyst surface and compare it to that of H_3PO_4. By using this approach, we were able to determine that the purity level as well as the time H_3PO_4 is stored after purification are important factors to be considered when gathering information about the catalyst´s activity and comparing them to literature values.

2. Experimental part

2.1. Chemicals and materials

Chemicals included $HClO_4$ 70 wt% (Fluka, ACS reagent), H_3PO_4 85 wt% (Sigma-Aldrich, 99.999 % trace metals basis), crystalline H_3PO_4 (Sigma-Aldrich, ≥99.999 % trace metals basis), anhydrous tetrahydrofuran (THF) (Sigma Aldrich, ACS reagent), isopropanol (Fluka, ACS reagent), H_2O_2 30 wt% (Sigma-Aldrich, ACS reagent), NaOH 1 mol dm^{-3} (reagent USP, Titripur). Both the Pt nanoparticles on Vulcan XC-72R carbon support and the 5 wt% solution of NS-5 Nafion were obtained from QuinTech.

2.2. H_3PO_4 purification

H_3PO_4 was purified using a standard procedure [13]: 200 cm^3 of a 85 wt% H_3PO_4 solution were placed in a 500 cm^3 perfluoroalkoxy alkane flask and 100 cm^3 of a 30 wt% H_2O_2 solution were added, resulting in formation of peroxyphosphoric acid which can oxidise the majority of impurities including the reduced phosphorus compounds. The solution was heated to 130 °C for 24 h, to allow peroxyphosphoric acid to be decomposed, until the majority of water had evaporated and the solution stopped boiling. The temperature was then increased to 165 °C for another 96 h to further concentrate the acid. The H_3PO_4 concentration was then determined by acid–base titration with a 0.1 mol dm^{-3} NaOH standard solution. H_3PO_4 was titrated as a monoprotic acid using methyl orange as pH indicator (2 drops of 0.5 g dm^{-3} methyl orange aqueous solution). 10 mL of H_3PO_4 (0.1 mol dm^{-3}) were titrated and the procedure was repeated 3 times for each H_3PO_4 solution (H_3PO_4 85 wt% before purification, H_3PO_4 crystalline and H_3PO_4 purified). It was not possible to quantify the traces of H_3PO_3 in the H_3PO_4 solutions since the concentration of H_3PO_3 is below the detection limit (NMR - see **Fig. S1**).

2.3. Pt/C catalyst characterisation

Thermogravimetric analyses (TGA) of the Pt/C catalyst were performed in an STA 449C Jupiter® analyser (NETZSCH). The sample was heated to 550 °C in an aluminium crucible at a rate of 10 °C min^{-1} in synthetic air. The Pt content in the catalyst was confirmed to be 31 ± 3 wt% (**Fig. S2**). The nanoparticles average diameter (2.3 ± 0.7 nm) was determined by transmission electron microscopy (TEM) (**Fig. S3**).

Brunauer-Emmett-Teller (BET) specific surface area measurements were performed by nitrogen adsorption/desorption at 77 K in a Micromeritics ASAP 2010 unit (Micromeritics). Prior to the measurements, the Pt/C catalyst was degassed for several hours at 80 °C to remove most of adsorbed water and other surface contaminants. The BET-determined surface area was found to be 159.8 ± 0.4 $m^2/g_{catalyst}$ (**Fig. S4**).

The electrochemical measurements were recorded on a VSP300 potentiostat with an EIS module (BioLogic). An AFMSRCE rotator (Pine Research) was used to control the rotation speed of the RDE.

2.4. Thin film (TF)-RDE preparation

The glassy carbon RDE tip (ø = 5 mm) was first polished with alumina particles of (average) size 0.3 μm and then with 0.05 μm particles. In either case, the particles were suspended in an alcoholic suspension (Buehler). The electrode was then sonicated in the presence of ethanol for 10 min, rinsed with ultra-pure water (18.2 MΩ

cm), sonicated for another 10 min, in ultra-pure water, and finally rinsed with ultra-pure water. The ink solution was prepared using 30 mg of Pt/C catalyst in 5 cm^3 of THF. The solution was sonicated for 25 min in an ice bath, then 0.1 cm^3 of 5 wt% Nafion solution were added to the ink and sonicated for 5 more minutes. 0.01 cm^3 of ink were then drop-casted onto the surface of the glassy carbon disc resulting in a catalyst loading of 97 μg_{Pt} cm^{-2}. The Pt/C thin film on the glassy carbon RDE tip was air dried by with rotating the tip at 700 rpm for 15 min.

2.5. Electrochemical setup and procedures

The electrochemical glass cell with an approximate volume of 660 cm^3 and water-jacket for heating was manufactured in-house (see Supplementary Information, **Fig. S5**). The glass components of the electrochemical cell were cleaned with piranha solution before using the cell for the first time. This was followed by boiling the cell in and rinsing it with ultra-pure Milli-Q water. Furthermore, the set-up was stored in Milli-Q water when not in use to avoid exposure to contaminants. The temperature during the experiments was set to 25 ± 2 °C. To optimize the electrolyte saturation with gas, the gas flow at the inlet was first directed through a frit to reduce the size of the bubbles. The counter electrode (CE) was a Pt coil inserted in a glass tube with a frit at the tip to prevent contamination of the electrolyte with products generated at the CE. The working electrode was either a commercial RDE (Pine Instruments, USA) with a glassy carbon disc (ø 5 mm) sheathed in a polytetrafluoroethylene cylinder or a polycrystalline Pt sheet electrode (99.99 % Pt, Safina) with geometric surface area of 1.2 cm^2 and roughness factor of 2.5, embedded in glass. A reversible hydrogen electrode (RHE, HydroFlex – Gaskatel) inserted into a Luggin capillary was used as a reference electrode in all experiments involving Pt/C. For consistency with experiments previously reported in the literature [12,27], $Hg|Hg_2SO_4|K_2SO_4$ (saturated) (0.654 V vs RHE at 25 °C) was used as a reference electrode during experiments with the polycrystalline Pt sheet electrode and the potential was corrected to that of RHE. All potential values in this paper are reported against RHE. The ohmic drop was compensated at 80 % using the current interrupt method, which left an uncompensated resistance of $\lesssim 5\ \Omega$ in the electrochemical cell. This remaining uncompensated resistance was corrected during data treatment.

2.5.1. Experimental procedures

The procedures described below were performed sequentially both for the stability tests and for measurements in different electrolytes. During the switching of electrolytes, the electrode was carefully washed with ultra-pure water and then kept imersed in the subsequent electrolyte to minimise exposure of the thin film to air.

Procedure 1 – TF-RDE preconditioning.

The procedure for TF–RDE preconditioning was performed in a stationary fashion by electrode potential cycling in 0.1 mol dm^{-3} $HClO_4$ electrolyte solution saturated with N_2. Scan description: +0.1 V → + 0.02 V → + 1 V → + 0.02 V, scan rate 0.100 V s^{-1}, number of cycles 100. This procedure is performed to electrochemically clean the catalyst surface off contaminants and to obtain a stable metallic surface.

Procedure 2 - ECSA determination via H_{upd}.

After catalyst preconditioning, the ECSA of the stationary electrode was determined via H_{upd} by performing cyclic voltammetry in the respective electrolyte solution under N_2 atmosphere. Scan description: +0.45 V → + 0.02 V → + 1 V → + 0.02 V, scan rate 0.020 V s^{-1}, number of cycles 3. The third scan was used for evaluation. The H_{upd} charge (Q_H) was obtained by integrating the current–time profile within limits corresponding to a potential region from + 0.02 V to + 0.43 V. The contribution of the double layer was subtracted in each specific electrolyte.

Procedure 3 - ORR activity.

The activity of the TF–RDE for ORR was evaluated using cyclic voltammetry in the respective electrolyte solution under electrode rotation (1600 rpm). Scan description: +1.1 V → + 0.4 V → + 1.1 V, scan rate 0.015 V s^{-1}, number of cycles 3. The third scan was used for evaluation.

First, the background currents for subtraction were obtained by measuring in an N_2–saturated solution. Then, O_2 was bubbled in the electrolyte solution for 20 min. The measurement was repeated while bubbling the O_2. The background current correction was performed by subtracting the voltammogram obtained in the presence of N_2 from the one obtained in the presence of O_2. The voltammogram in the direction from + 1.1 V → + 0.4 V was plotted and analysed.

Procedure 4 - ECSA determination via CO stripping.

In the next step, the ECSA of the stationary electrode was determined via CO stripping by performing cyclic voltammetry in the respective electrolyte solution. Before starting the CO stripping procedure, a cyclic voltammogram was recorded in an N_2-saturated electrolyte, to be used as the background. Scan description: +0.1 V → + 0.02 V → + 1.1 V → + 0.02 V, scan rate 0.020 V s^{-1}, number of cycles 3. After acquiring the background signal, CO was bubbled concurrently with the application of + 0.1 V for 4 min, enough for the CO to adsorb on the Pt surface. This potential value was similar to the one used by Rudi et al. [26], who have previously optimized the procedures for ECSA determination with RDE. In the next step, the CO present in the electrolyte solution was purged by bubbling N_2 for 20 min, leaving behind only the CO adsorbed on the Pt surface. For CO stripping, a cyclic voltammogram was recorded. Scan description: +0.1 V → + 1.1 V → + 0.02 V → + 1.1 V, scan rate 0.020 mV s^{-1}, number of cycles 3. The first scan was used for evaluation. When determining H_3PO_3 adsorption isotherms at Pt/C via CO stripping, the starting potential was changed to 0.45 V. This potential was chosen as the maximum Pt surface coverage with H_3PO_3 occurs at this potential value, due to absence of H_{upd} [12]. At the same time, this potential is still sufficiently low to avoid any undesired oxidation of H_3PO_3 and CO. The second cycle was always used for background current subtraction.

2.5.2. Experiments

Stability test

The stability test was performed with a 0.1 mol dm^{-3} $HClO_4$ electrolyte. First of all, one freshly prepared TF–RDE (with Pt/C catalyst) labelled as "TF–RDE (1)" was preconditioned (*Procedure 1*). Then, a sequence consisting of *Procedure 2 (ECSA determination via H_{upd}), Procedure* 3 (*Oxygen reduction reaction kinetics*) *and Procedure 4 (ECSA determination via CO stripping)* was performed in 0.1 mol dm^{-3} $HClO_4$ solution. The sequence of these three procedures will be referred to as the "cycle". This cycle was repeated 3 times. The stability test was repeated 3 times (**Fig. S10**).

Measurements using different electrolytes.

To verify the influence of phosphoric acid purification on the performance of Pt/C catalysts, sequential measurements were made with another freshly prepared and preconditioned (*Procedure 1*) TF–RDE (with the Pt/C catalyst), labelled as "TF–RDE (2)", using the following sequence of electrolytes:

1^{st} & 2^{nd} – 0.1 mol dm^{-3} $HClO_4$,
3^{rd} – 0.1 mol dm^{-3} $HClO_4$ + 0.1 mol dm^{-3} crystalline H_3PO_4,
4^{th} – 0.1 mol dm^{-3} $HClO_4$ + 0.1 mol dm^{-3} purified H_3PO_4,
5^{th} – 0.1 mol dm^{-3} $HClO_4$ + 0.1 mol dm^{-3} non-purified H_3PO_4,
6^{th} – 0.1 mol dm^{-3} $HClO_4$.

2.6. H_3PO_3 adsorption isotherms

Before starting the isotherm measurements, a new TF-RDE with Pt/C catalyst, labelled as "TF-RDE (3)" was preconditioned as described in *Procedure 1*. The determination of H_3PO_3 adsorption on the catalyst was based on measuring the Pt ECSAs by H_{upd} and CO stripping tech-

niques (as described in the previous sections) in various electrolyte solutions. The ECSAs were first determined in 0.1 mol dm^{-3} $HClO_4$. Then, the measurement was repeated in the solution containing a gradually increasing amount of H_3PO_3. After each addition of H_3PO_3, the electrolyte solution was bubbled with N_2, the electrode was rotated at 2000 rpm for 5 min to homogenise the solution, and then H_{upd} and CO stripping routines were performed.

3. Results and discussion

3.1. Benchmarking Pt/C-based TF–RDE behaviour in $HClO_4$ (stability test)

TF-RDEs were prepared with Pt/C catalyst as described in the experimental section. ECSA (H_{upd} and CO stripping methods) and ORR activity were studied in various electrolytes, as shown in Fig. 1. The rotational air-drying method used as described earlier for TF-RDE preparation offers a higher reproducibility than stationary air drying. However, it still does not allow for a direct comparison of different TF-RDEs in terms of their absolute ECSA values [28]. Moreover, ECSA measurements are very sensitive to any changes resulting from the electrode's history, i.e. number of cycles, potential window selected, etc. Therefore, five stability cycles were performed in 0.1 mol dm^{-3} $HClO_4$ solution with TF–RDE (1). The purpose of this particular sequence was to determine the extent of changes in ECSA and ORR activity that results when the above-defined cycles were performed in 0.1 mol dm^{-3} $HClO_4$ solution. This serves as a baseline for the rigorous experiments where the supporting electrolyte solution composition were changed. As can be seen from voltammograms in Fig. 1**A, B and C**, the most significant (but still minor) changes of the electrochemical behaviour of the Pt/C catalyst occur between cycles 1 and 2. In particular, these minor changes involve:

- A decrease in adsorption/desorption peak currents in both the H_{upd} and the Pt oxidation/$PtO(H)_{ads}$ reduction region in Fig. 1**A**,
- A slight shift of ORR towards higher electrode potentials in Fig. 1**B** and
- A minor shift of CO stripping peak towards lower electrode potentials in Fig. 1**C**.

No further changes in the characteristics of Pt/C voltammograms were observed. The ECSA determined by both techniques decreased nearly linearly with the increasing cycle number, see Fig. 1**D**. The original ECSA obtained by CO stripping ($ECSA_{CO}$) was about 27 % higher than that determined by H_{upd} ($ECSA_H$). On the other hand, the decrease in $ECSA_{CO}$ was faster (7 % per cycle) than that of $ECSA_H$ (4 % per cycle). Determining the exact origin of these differences and changes is out of the scope of the present work, but they might be related to the different adsorption energies of different adsorbates at the Pt surface, or they could be related to a surface-level restructuring of nanoparticulate Pt in the thin film upon polarization [26]. Finally, it is interesting to note that the geometric-area-based ORR current density does not change despite the fact that a significant reduction in ECSA was observed.

3.2. Effect of H_3PO_4 purity on Pt/C-based TF–RDE behaviour

Analogous measurements to the ones performed for benchmarking the changes in the Pt/C catalyst during stability cycles in 0.1 mol dm^{-3} $HClO_4$ environment were performed using TF–RDE (2) with the electrolyte solutions being changed sequentially. To stabilise the response of TF–RDE (2), the first two measurement cycles were performed in 0.1 mol dm^{-3} $HClO_4$, the results of which are presented in Fig. 2**A, B and C**.

The extent and nature of the changes observed within these two first cycles were similar to the ones observed during the stability test discussed in section 3.1. The following cycles, i.e. cycles no. 3 to 5, were performed with solutions containing both 0.1 mol dm^{-3} $HClO_4$ and 0.1 mol dm^{-3} H_3PO_4 of various purities, as described in section 2.5.2. In particular, H_3PO_4 purity decreased with increasing cycle number, i.e. crystalline (cycle no. 3), purified (cycle no. 4) and non-purified H_3PO_4 (cycle no. 5). Long-term storage of the acid after the purification process is expected to result in a negative impact on performance due to the absorption of impurities from the environment and/or from the container. Hence, it is recommended that long-term storage of H_3PO_4 solutions after purification is avoided.

As shown in Fig. 2**A**, the addition of H_3PO_4 into the electrolyte solution caused a decrease of the current response over the whole investigated potential range of Pt/C voltammograms except for the double layer region. Peaks at 0.25 and 0.1 V in the reduction part of the H_{upd} region and related oxidation peaks became sharper. At the same time, the onset of Pt oxide formation shifted by about 0.1 V to more positive electrode potentials. This is a typical behaviour observed in an H_3PO_4 environment ascribed to the adsorption of H_3PO_4 and/or its anions on the Pt surface [12,27,29]. The purity of H_3PO_4 did not seem to have a significant effect on the profile of the voltammograms.

When comparing the ORR activity in **Fig. 2B**, a reduction in Pt/C activity in the presence of H_3PO_4 was observed. This is documented by a shift of the voltammograms by about 0.1 V to lower electrode potential values. However, it seems that the purity level of the H_3PO_4 does not play a strong role in the Pt/C activity towards ORR. A slight reduction in ORR limiting current density is also visible with the smallest limiting current being observed in the case of non–purified H_3PO_4. The CO oxidation peak profile changed only in the presence of non-purified H_3PO_4, where an additional pronounced oxidation peak became apparent just before the standard CO stripping peak at 0.8 V, see Fig. 2**C**. A detailed view of the CO stripping peaks showing the small prepeak around 0.65 V, which can be attributed to increased step defects on Pt surface [30,31], is shown in **Fig. S8** in Supplementary information. When a final cycle (no. 6) was performed, again in 0.1 mol dm^{-3} $HClO_4$, all the recorded profiles again resembled the ones observed in cycles no. 1 and 2. The change of $ECSA_{CO}$ and $ECSA_H$ over each cycle is summarized in Fig. 2**D** and exact values are included in Table 1.

The decrease of ECSAs, which is visible between cycles no. 1 and 2 (in 0.1 mol dm^{-3} $HClO_4$), closely resembles the trends found during the stability test. When crystalline and purified H_3PO_4 were introduced in the electrolyte solution (cycles no. 3 and 4), the decrease in $ECSA_{CO}$ remains practically constant. However, the presence of non–purified H_3PO_4 during cycle no. 5 led to the most significant drop in $ECSA_{CO}$. Interestingly, replacing the solution with a 0.1 mol dm^{-3} $HClO_4$ solution (cycle no. 6) led the $ECSA_{CO}$ to increase to the level expected on the basis of the stability test (1 % decrease compared to the expectations based on the stability test, see full and empty squares in Fig. 2**D**). The situation with $ECSA_H$ was somewhat different, since using crystalline H_3PO_4 in cycle no. 3 already caused a dramatic reduction of the $ECSA_H$ value (8 % drop compared to the expectations based on the stability test, see full and empty circles in Fig. 2**D**). On the other hand, exchanging crystalline H_3PO_4 with purified H_3PO_4 slowed down the $ECSA_H$ decay rate to a similar level as seen with the $HClO_4$ solution. This is documented by the same slopes of the $ECSA_H$ drops between cycle no. 3 and 4 during the stability test and experiments with different electrolytes. The $ECSA_H$ decrease, determined in non–purified H_3PO_4, was again significantly higher. Final measurements performed in a 0.1 mol dm^{-3} $HClO_4$ solution revealed a decrease in $ECSA_H$ similar to that in the stability experiment. However, the absolute $ECSA_H$ values remained rather low and by no means did they recover as in the case of $ECSA_{CO}$. This may indicate that parts of the hydrogen adsorption sites are permanently compromised after exposure to different electrolytes and by repeated electrochemical measurements. An additional source of errors could be the subtraction of overestimated charging currents as discussed in the Introduction.

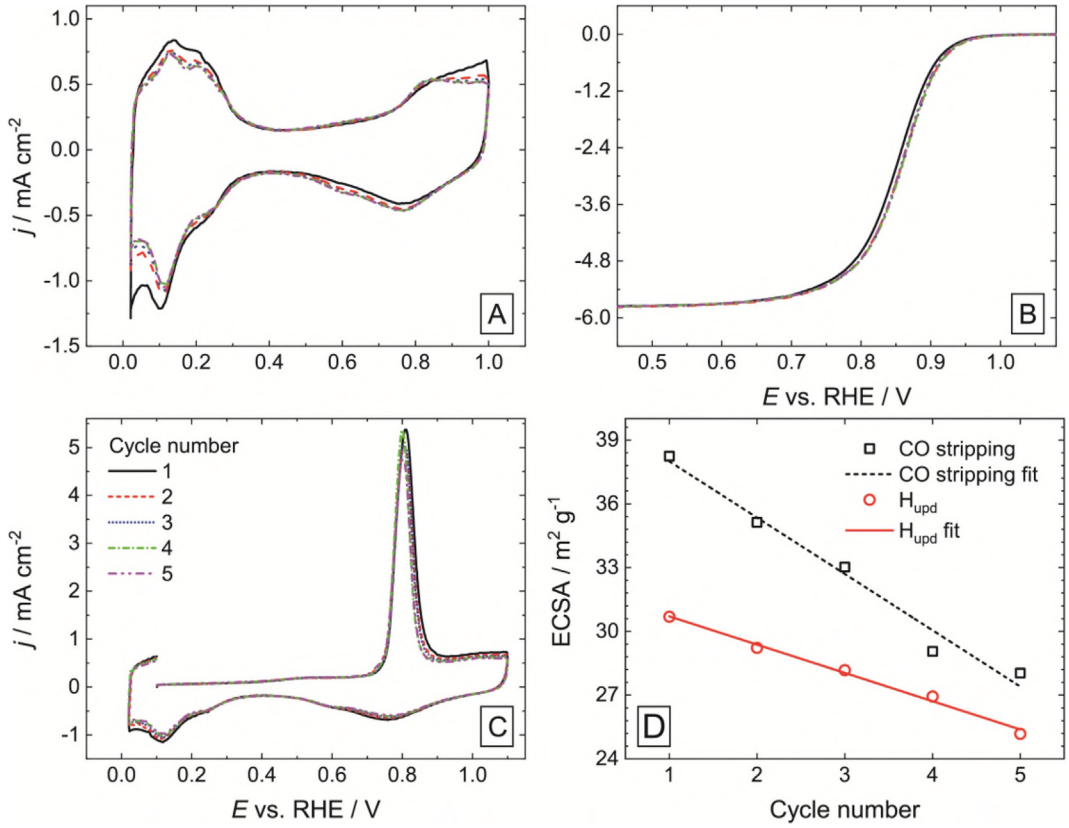

Fig. 1. (**A**) Cyclic voltammograms performed under N_2 atmosphere, at a potential sweep rate of 20 mV s^{-1} and at 0 rpm. Cycle number 3 is shown. (**B**) ORR activity measured using CV, only the anodic direction is shown. The background contribution (CV obtained in N_2) was subtracted from the ORR curve. The measurements were performed under O_2 atmosphere, at potential sweep rate of 15 mV s^{-1} and at 1600 rpm. (**C**) CO stripping voltammograms. The measurements were performed under N_2 atmosphere, at potential sweep rate of 20 mV s^{-1} and at 0 rpm. Cycle number 1 is shown. **(D)** ECSA determined via H_{upd} and CO stripping as a function of the cyclic voltammetry cycle, ($ECSA_{Hupd} = (32.0 \pm 0.2)m^2g_{Pt}^{-1} + (-1.3 \pm 0.1)m^2g_{Pt}^{-1} \times$ Cycle no.) and ($ECSA_{CO\ stripping} = (40.6 \pm 0.8)m^2g_{Pt}^{-1} + (-2.7 \pm 0.2)m^2g_{Pt}^{-1} \times$ Cycle no.). The stability test was repeated 3 times and the other replicates can be seen in Fig. S10. For all of these electrochemical measurements, TF–RDE (1) was used. Measurements were performed using 0.1 mol dm^{-3} $HClO_4$ electrolyte solution. Cycle numbers are provided in the legend of fig. C.

At this point, it is worth looking in more detail at the ORR kinetics. Before analysis, all ORR voltammograms presented in Fig. 1**B** and Fig. 2**B**, were corrected for the mass transport limitation in the electrolyte solution using the classical formula (Equation (2)) derived from the Koutecky–Levich equation.

$$j_{kin} = \frac{j \cdot j_{lim}}{|j_{lim} - j|} \tag{2}$$

here j_{kin} represents the kinetic current density at a given electrode potential (E), j_{lim} is the limiting current density and j is a current density at any given E. Two Tafel slopes were found on selected polarisation curves presented in the form $\log(j_{kin}) = f(E)$, see Supplementary information (**Fig. S7**). The first Tafel slope can be observed in the low current density region corresponding to the potential range from 1 to 0.85 V, where the Pt surface is expected to be, at least partly, covered by oxides/adsorbed O [32,33]. The second Tafel slope is present in the high current density region in the potential range from 0.77 to 0.55 V, which correlates with the double layer region, where the Pt surface should be free of oxides/adsorbed O [32,33]. The kinetic parameters determined from cycles no. 2–5 for ORR in 0.1 mol dm^{-3} $HClO_4$ are summarised in the Supplementary information (**Table S1**). Kinetic parameters determined in cycle no. 1 were not considered, since they differ from those found for theremaining cycles. It can be seen that in the low current density region, the Tafel slope and j_0 are about − 58 mV dec^{-1} and $2.6 \cdot 10^{-6}$ mA cm^{-2}, respectively. Such Tafel slope value is in good agreement with numerous previous works corresponding to electrodes where part of the Pt surface is covered by oxygen adsorbates [34]. The values of the Tafel slope and j_0 in the high current density region, however, were significantly higher than other literature values (−186 mV dec^{-1} and 0.65 mA cm^{-2}, respectively). Such high current density region value of Tafel slope is higher than the usual −120 mV dec^{-1} reported for polycrystalline Pt electrodes and as explained by other theoretical works reported in literature [35,36]. It has been suggested that a Tafel slope (in absolute value) higher than −120 mV dec^{-1} is, in this case, a result of limited O_2 mass transport within a catalytic layer [37]. On the other hand, a similar Tafel slope value was reported for Pt nanoparticle arrays without a catalytic layer in the potential region below 0.7 V [38]. In this case, however, the mass transport limitation is less likely. In any case, although it is not clear if the Tafel slope value of −186 mV dec^{-1} determined in our experiments has a direct microkinetic meaning, it is still useful when discussing an effect of impurities, which is the main goal of this work. A more detailed analysis of the kinetic data can also be found in literature [35,39,40]. It has to be mentioned here that the precision of the determined kinetic constants in the high current density region is low due to a significant extent of current density correction, which is required at low electrode potentials where j values start to approach j_{lim}. This is also indicated by a higher standard deviation of the kinetic parameters in the high current density region. In any case, an increase in j_0 when going from low to high current density region by nearly-five

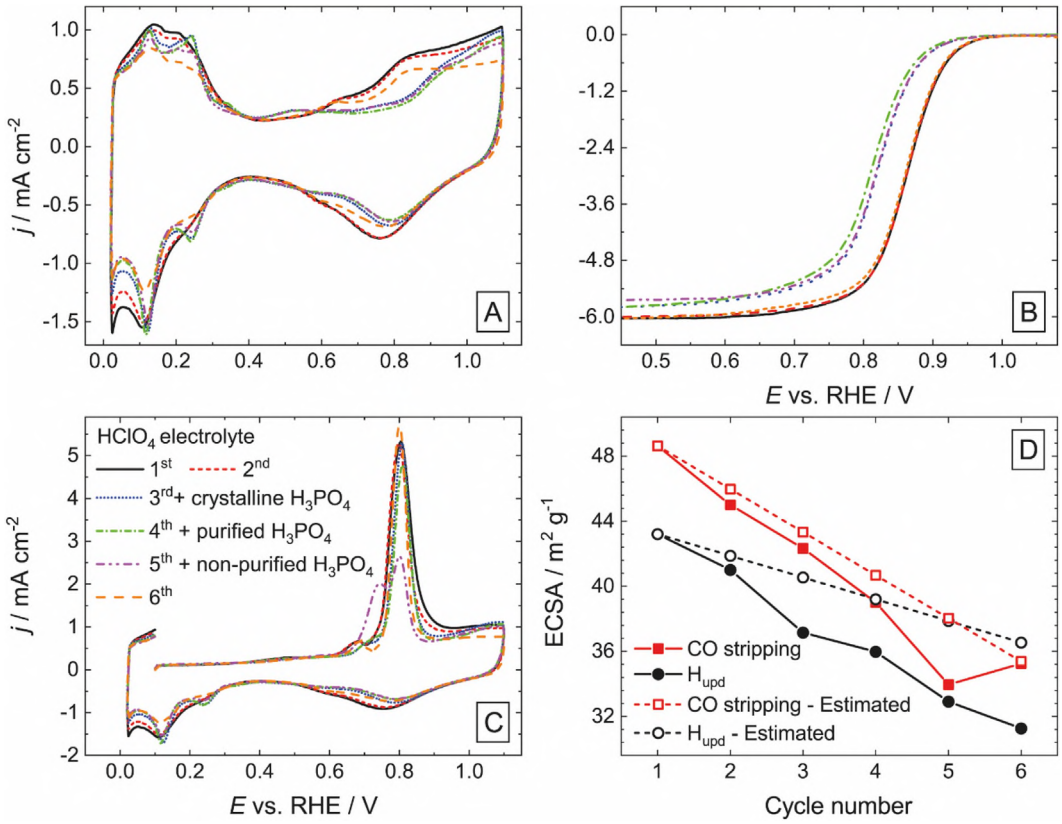

Fig. 2. (**A**) Cyclic voltammograms performed under N_2 atmosphere at a potential sweep rate 20 mV s^{-1} and at 0 rpm; the cycle number 3 is shown. (**B**) ORR activity measured using CV, only the anodic direction is shown. The measurements were performed under O_2 atmosphere, at a potential sweep rate of 15 mV s^{-1} and at 1600 rpm. (**C**) CO stripping cyclic voltammograms were performed under N_2 atmosphere, at a potential sweep rate of 20 mV s^{-1} and at 0 rpm. (**D**) ECSA determined via H_{upd} and CO stripping versus cycle repetition and ECSA curve estimated using the linear fit shown in Fig. 1**D**. For these electrochemical measurements, the same thin film of Pt/C was used, using different electrolytes. Cycles 1, 2 and 6 were performed in $HClO_4$ 0.1 mol dm^{-3}, measurements 3 to 5 in mixtures of 0.1 mol dm^{-3} $HClO_4$ + 0.1 mol dm^{-3} H_3PO_4. The latter is prepared from H_3PO_4 sources of the following purity levels: crystalline (cycle no. 3), purified (cycle no. 4), and non-purified (cycle no. 5), respectively.

Table 1
ECSA as determined by H_{upd} and CO stripping methods using different electrolytes.

Electrolyte –	Cycle –	$ECSA_{Hupd}$ $m^2\ g^{-1}$	$ECSA_{CO}$ $m^2\ g^{-1}$
$HClO_4$	1	43	49
$HClO_4$	2	41	45
$HClO_4$ + H_3PO_4 crystalline	3	37	42
$HClO_4$ + H_3PO_4 purified	4	36	39
$HClO_4$ + H_3PO_4 non-purified	5	33	34
$HClO_4$	6	31	35

orders of magnitude was observed. A pronounced difference of several orders of magnitude between j_0 obtained in these two regions has been well established in literature, e.g. [41,42]. which is attributed to the inhibiting effect of oxygen species at the Pt surface [43]. The increase of the Tafel slope could be explained by a change in the surface composition, rate-determining step or even the reaction mechanism of the ORR [7,44].

Kinetic parameters determined for sample TF–RDE (2) are summarised in the Supplementary information (**Table S2**). The Tafel slope and j_0 in the low (–0.058 V, $3.0{\cdot}10^{-6}$ mA cm^{-2}) and high current density (–0.202 V, 0.42 mA cm^{-2}) region in 0.1 mol dm^{-3} $HClO_4$ solution (cycle no. 2) are close to those observed for the previous TF–RDE (1) in the same electrolyte solution. Regardless of its purity, the presence of H_3PO_4 in the solution caused only a minor increase of the low current density Tafel slope to approximately –0.065 mV dec^{-1} and j_0 values changes were negligible and within experimental precision. More interesting changes were observed, however, in the high current density region. Here, the introduction of crystalline and purified H_3PO_4 did not cause any visible changes to the Tafel slope, but j_0 decreased by about 65 %. In the presence of non–purified H_3PO_4 the Tafel slope decreased to about –0.140 mV dec^{-1} and j_0 dropped by as much as 95 %. This suggests that a significant portion of the active sites are blocked by species other than H_3PO_4. The Tafel parameters determined for the last cycle (no. 6), which was performed again in a 0.1 mol dm^{-3} $HClO_4$ solution, almost returned to their original values (as observed in cycle no. 2 before the addition of H_3PO_4).

The experimental results seem to suggest that the electrolyte composition also affects the limiting current (j_{lim}), since values decrease by about 3.5 % and 6 % after addition of crystalline or purified (cycle no. 3 and 4) H_3PO_4 and non–purified (cycle no. 5) H_3PO_4 into the 0.1 mol dm^{-3} $HClO_4$ solution, respectively. Finally, the j_{lim} value observed during the final cycle (no. 6) performed in $HClO_4$ solution is the same as in cycle no. 2.

These observations can be explained by the following considerations: H_3PO_4 and/or its anions are known to adsorb at the Pt surface and significantly reduce the amount of oxygen-containing adsorbates. Their interactions with Pt surfaces have already been discussed elsewhere [7]. In summary, $H_2PO_4^-$ exhibits maximum coverage of the Pt surface at potentials corresponding to the double layer region, where the co-adsorption of H or O on $H_2PO_4^-$ is absent. In a first approximation, crystalline and purified H_3PO_4 exert the very same

effect on the behaviour of the Pt/C catalyst present in the TF–RDE for all of the above investigated cases ($ECSA_H$, $ECSA_{CO}$, ORR). Since these H_3PO_4 sources are highly pure and do not contain measurable amounts of contaminants, their effect can be attributed solely to the action of H_3PO_4 and/or its anions. On the other hand, non–purified H_3PO_4 negatively influenced $ECSA_H$, $ECSA_{CO}$, ORR kinetic parameters in the high current density region, and j_{lim} of ORR. These observed changes can be attributed to the interaction between strongly adsorbing species (that can be removed with H_2O_2), contained in non–purified H_3PO_4, and the catalyst centres. We believe that the main contaminant is H_3PO_3. A schematic showing the hypothesised effect of H_3PO_3 on the ORR at Pt electrodes is presented in Fig. 3.

In particular, the competition between H_3PO_3 and hydrogen atoms in H_{upd} for adsorption sites, described in our previous works [12,27], explains well the observed drop in $ECSA_H$ to a level below that observed in the presence of crystalline and purified H_3PO_4 in the present work. In this context, it is necessary to mention that H_3PO_3 is not oxidised at a measurable rate in the H_{upd} potential range. The significant drop in $ECSA_{CO}$ and changes in the CO stripping voltammogram in the presence of non-purified H_3PO_4 as shown in Fig. 2**C** can be explained analogously. First of all, it is good to keep in mind that CO adsorption was performed at 0.1 V, i.e. well within the H_{upd} potential region. In addition to that, the appearance of the oxidation peak at 0.75 V just before the CO stripping peak in non-purified H_3PO_4, can be attributed (as will be shown later) to the anodic oxidation of H_3PO_3. From the above description of the ORR kinetic results, it follows that in the low current density region (potential ranging from 1 to 0.85 V) the kinetic parameters were not affected by the impurities present in non–purified H_3PO_4. On the other hand, in the high current density region of ORR (potential ranging from 0.77 to 0.55 V) both the Tafel parameters were influenced significantly. This difference can be attributed to the fact that in the first scenario (high positive potentials), H_3PO_3 is immediately oxidised at the Pt surface with adsorbed oxygen-containing intermediates (e.g. $(OH)_{ads}$ or O_{ads}, denoted here shortly as PtO_x). Therefore, the surface concentration of H_3PO_3 on the Pt/C surface is close to zero. On the other hand, at the lower potentials (in the high current density region of ORR) H_3PO_3 partially accumulates at the Pt surface and influences the ORR kinetics. This likely H_3PO_3 accumulation at the Pt/C surface is in accordance with a 95 % drop in the high current density j_0 value.

Additional insights can be gained by looking at the j_{lim} values, which are, at any given temperature, directly proportional to the solubility of O_2. Furthermore, O_2 solubility in the electrolyte solution is also influenced by the ionic strength of the electrolyte (the so–called salting out effect), which has to be considered when analysing the j_{lim} values. Therefore, based on the work of Weisenberger et al. [45] the O_2 solubility in a 0.1 mol dm^{-3} $HClO_4$ + 0.1 mol dm^{-3} H_3PO_4 solution was calculated to be 2 % lower than in a 0.1 mol dm^{-3} $HClO_4$ solution. This suggests that the additional j_{lim} drop by 1.5 % in the presence of crystalline or purified H_3PO_4 is caused by partial Pt/C surface blocking by H_3PO_4 and/or its anions. A further 2.5 % drop in j_{lim} value in non–purified H_3PO_4 can be assigned to H_3PO_3 adsorption at the Pt/C surface. In summary, the largest effect of H_3PO_3 on the processes at the Pt surface can be expected in the potential region between H_{upd} (at H_{upd} potentials the adsorbed H_3PO_3 is at least partially replaced by adsorbed H) [12] and the potential where the anodic oxidation of H_3PO_3 starts to occur at a measurable rate.

The co-adsorption of H_3PO_3 and $H_2PO_4^-$ on a Pt surface in aqueous electrolytes represents a complex issue, rendering determination of H_3PO_3 adsorption isotherms in H_3PO_4 electrolyte problematic. It is clear that the adsorption of H_3PO_3 on Pt is stronger and, most probably, not simple physisorption as in the case of $H_2PO_4^-$. In order to assess the impact of $H_2PO_4^-$ on an ECSA of Pt determined by H_{upd} and CO stripping procedures, it is convenient to shift to a less complex system of a bulk polycrystalline Pt electrode. This enables observing changes in voltammogram shapes and ECSA of Pt due to CO-$H_2PO_4^-$ interaction and direct comparison of these results with H_{udp}.

3.3. H_3PO_3 isotherm on Pt/C

As mentioned in the previous section, the co-adsorption of $H_2PO_4^-$ and CO can potentially lead to significant differences in ECSA values determined by CO stripping and H_{upd} methods. In addition, results obtained previously in Section 3.2 implied that the purity of H_3PO_4 has a significant impact on the determined values of Pt ECSA. To evaluate the effect of H_3PO_4 concentrations on both ECSAs in more detail, a series of experiments was performed on a simplified system, i.e. polycrystalline bulk Pt electrode using additions of the crystalline H_3PO_4 to deaerated 0.5 mol dm^{-3} $HClO_4$ electrolyte. The concentration of $HClO_4$ was chosen in order to be consistent with our previous results obtained on a bulk Pt electrode [12,27]. The results of these experiments are summarised in Supplementary Information. These results clearly pointed out that co-adsorption of $H_2PO_4^-$ and CO does not result in a significant change of polycrystalline bulk Pt ECSA and results of CO stripping and H_{upd} methods performed in aqueous electrolytes of H_3PO_4 are similar. Therefore, it was possible to introduce the H_3PO_3 to the Pt/C-H_3PO_4 system in the next step.

Both H_{upd} and CO stripping voltammograms at Pt/C were recorded in 0.1 mol dm^{-3} $HClO_4$ and in 0.1 mol dm^{-3} $HClO_4$ + 0.1 mol dm^{-3} H_3PO_4. As already described [12,27], increasing H_3PO_3 concentration within the $HClO_4$ solution leads to, regardless of the H_3PO_4 presence in the electrolyte solution, the gradual disappearance of ad/desorption peaks in the H_{upd} region, increase of oxidation currents at potentials above 0.55 V and finally, the disappearance of Pt oxide reduction peaks during scanning towards negative potentials (see Fig. 4**A**). The oxidation peaks with a maximum at about 0.75 V (onset potentials are not affected by the presence of H_3PO_4, see voltammograms in Fig. 4 **A** and **C**) can be attributed to the anodic oxidation of H_3PO_3 to H_3PO_4 at the Pt surface. It is worth mentioning here that the presence of H_3PO_3 in $HClO_4$ solution in concentrations below 0.1 mmol dm^{-3} have an effect that can hardly be observed at all in the voltammograms in Fig. 4**A and C**. This is in sharp contrast to CO stripping voltammograms presented in Fig. 4**B and D** where the presence of H_3PO_3 in concentrations as low as 1.6×10^{-2} mmol dm^{-3} causes a visible decrease of the CO stripping peak current density (peak potential of about 0.8 V). At the same time, a new oxidation peak (with maximum at about 0.74 V) starts to appear just before the CO stripping peak. This is clearly visible on voltammograms recorded in solution with H_3PO_3 at concentrations of around 7×10^{-2} mmol dm^{-3}. The oxidation peak potential of about 0.74 V coincides with the potential of anodic oxidation of H_3PO_3 to H_3PO_4. Interestingly, a practically identical voltammogram was observed in the case of CO stripping in 0.1 mol dm^{-3} $HClO_4$ with non-purified H_3PO_4, as discussed above (not shown), suggesting a similar composition of both electrolyte solutions. This observation allows us to roughly assume that the H_3PO_3 concentration in the 0.1 mol dm^{-3} H_3PO_4 solution was also about 0.07 mmol dm^{-3}, i.e. that the molar ratio between H_3PO_3 and H_3PO_4 is approximately 7×10^{-4}. Further increasing the H_3PO_3 concentration to about 1.7 mmol dm^{-3} causes the CO stripping peak to disappear, suggesting that H_3PO_3 adsorbs concurrently and blocks the majority of CO from the Pt surface. At even higher H_3PO_3 concentrations, the H_3PO_3 oxidation peak broadens and shifts to higher electrode potentials and the CO stripping voltammograms (Fig. 4**B and D**) resemble those obtained in the absence of CO (Fig. 4**A and C**). Also, in this case, the presence of H_3PO_4 in the electrolyte solution does not affect the observed behaviour; see Supplementary Information (**Fig. S9**).

Where possible, the Q_H and Q_{CO} values were determined using the voltammograms discussed above. Firstly, using the Q_H values, H_3PO_3 adsorption isotherms at Pt/C catalyst presented in Fig. 5**A** were calcu-

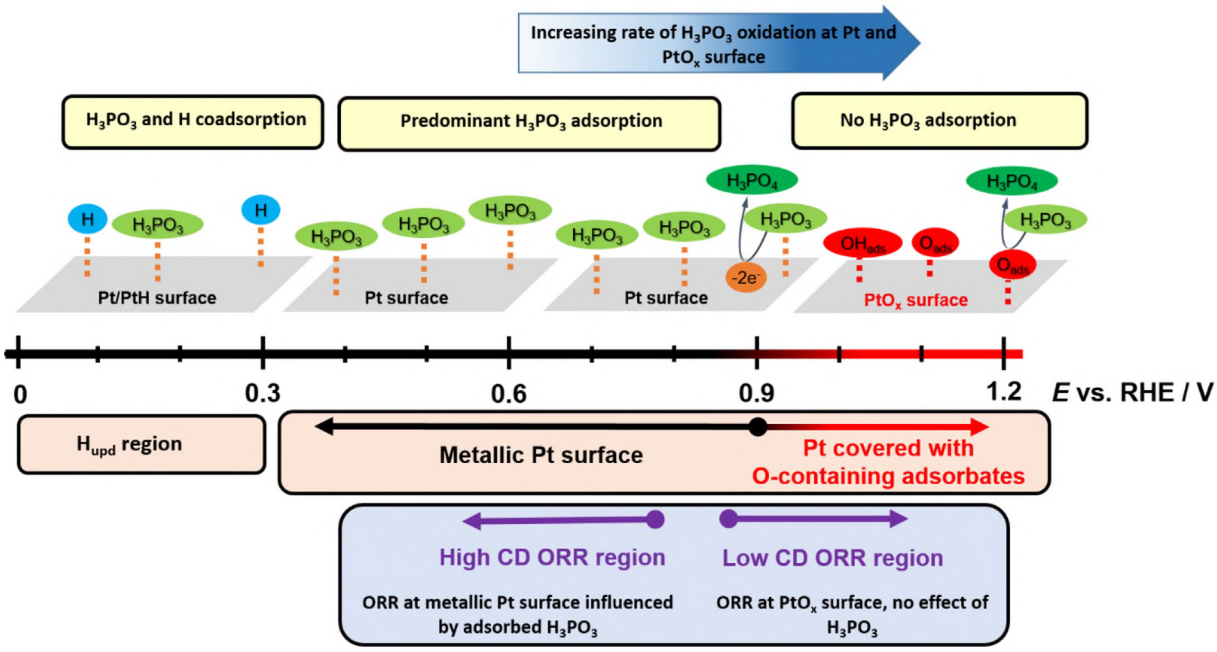

Fig. 3. Schematics showing the theoretical effect of H_3PO_3 on the ORR reaction ocurring on Pt electrodes at 25 °C.

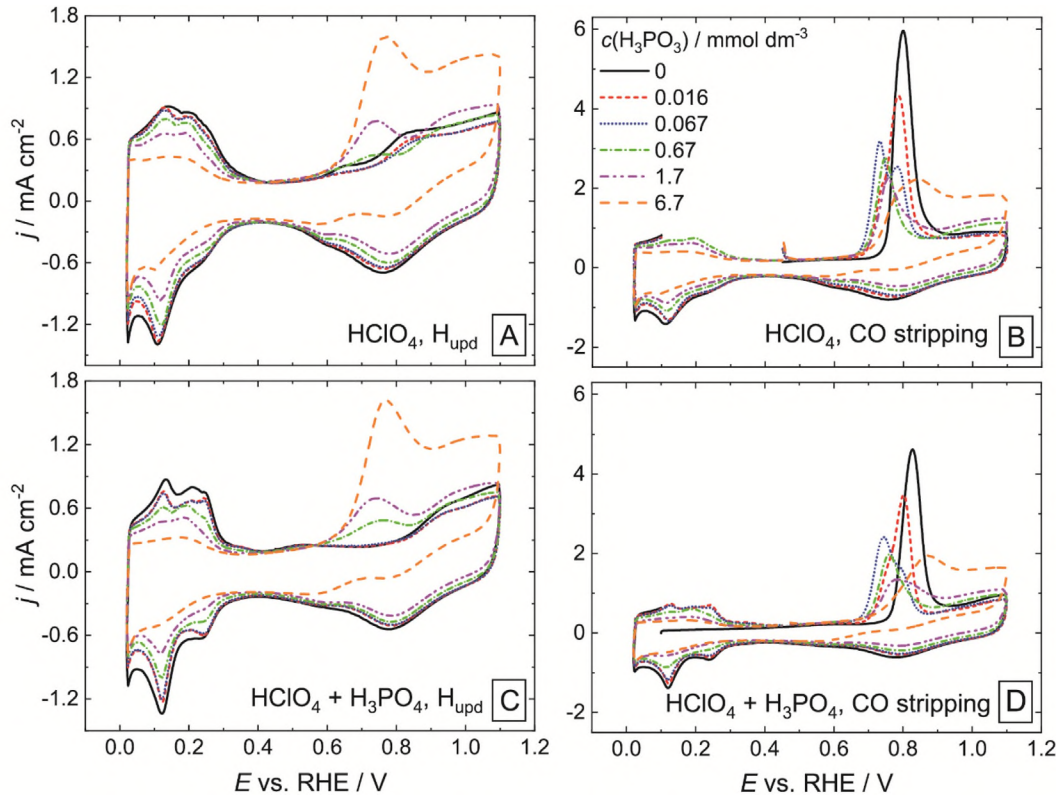

Fig. 4. (**A**) and (**C**): Cyclic voltammograms obtained under N_2 atmosphere, at a potential sweep rate of 20 mV s^{-1} and at 0 rpm, cycle number 3 is shown; (**B**) and (**D**): CO stripping voltammograms obtained under N_2 atmosphere, at a potential sweep rate of 20 mV s^{-1} and at 0 rpm. These data were used to build the H_3PO_3 adsorption isotherms at a temperature of 25 ± 2 °C on a Pt/C thin film in 0.1 mol dm^{-3} $HClO_4$ (**A** and **B**) and in a mixture containing 0.1 mol dm^{-3} $HClO_4$ and 0.1 mol dm^{-3} H_3PO_4 (crystalline) (**C** and **D**).

lated by means of Equation (3). While the Pt surface coverage by H_3PO_3 in 1×10^{-3} mmol dm^{-3} H_3PO_3 solution remains relatively low (about 10 %), 70 % of the Pt surface is covered by H_3PO_3 when using the 6.7 mmol dm^{-3} H_3PO_3 solution. In the majority of the concentration range, the presence of H_3PO_4 seems to increase the surface coverage by about 5 %. The isotherm obtained via H_{upd} showed a behaviour very similar to that obtained for the polycrystalline Pt foil in our previous works [12,27].

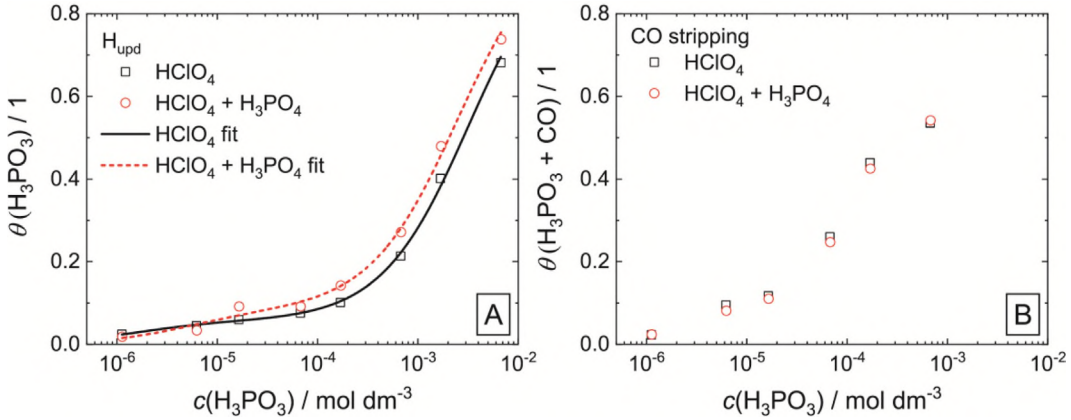

Fig. 5. H_3PO_3 adsorption isotherms at a temperature of 25 ± 2 °C on a Pt/C thin film in (**A**) 0.1 mol dm^{-3} $HClO_4$ and (**B**) 0.1 mol dm^{-3} $HClO_4$ + 0.1 mol dm^{-3} H_3PO_4 (crystalline). θ is the partial surface occupation by H_3PO_3, calculated by Equation (3).

Due to the incompatibility between the CO stripping voltammograms and corresponding backgrounds at higher H_3PO_3 concentrations, it was not possible to determine Q_{CO} values at H_3PO_3 concentrations exceeding 6.7×10^{-4} mol dm^{-3}. This is likely the consequence of the fact that increasing amounts of H_3PO_3 oxidised at the Pt surface originate from the electrolyte bulk and not from the electrode | electrolyte interface (adsorbed H_3PO_3). As has already been discussed, the oxidation currents observed in the CO stripping voltammograms in the potential range between 0.6 and 0.9 V (Fig. 4**B and D**) are a consequence of both H_3PO_3 and CO oxidation, both of which require two electrons to be completely oxidated. Therefore, a simple equimolar replacement of CO by H_3PO_3 should not lead to changes in Q_{CO} values. Consequently, the curves presented in Fig. 5**B** should be interpreted as mixed (H_3PO_3 + CO) adsorption isotherms. The fact that increasing H_3PO_3 concentration leads to lower Q_{CO} suggests either that CO and/or H_3PO_3 are not fully oxidised when both are present at the Pt surface or, what is more likely, that repulsive lateral interactions exist between H_3PO_3 molecules as well as between H_3PO_3 and CO molecules at the Pt surface. An alternative explanation is that adsorbed H_3PO_3 molecules would interact with more than one surface Pt atom. This is partially in contradiction with multilayer adsorption of H_3PO_3 observed previously [12]. However, previous results were obtained using a different methodology, in lower potential range at around 0.4 V vs RHE and at the Pt sheet electrode.

$$\theta = \frac{\left(Q_{\mathrm{Pt\,HClO_4\,(+H_3PO_4)}}\right) - \left(Q_{\mathrm{Pt\,HClO_4\,(+H_3PO_4)+H_3PO_3}}\right)}{\left(Q_{\mathrm{Pt\,HClO_4\,(+H_3PO_4)}}\right)} \quad (3)$$

In this equation, θ (dimensionless) is the partial surface occupation by H_3PO_3.

Finally, the H_3PO_3 isotherms were fitted using the Origin Pro software using the double Langmuir adsorption model as in Equation (4), which has been previously, and successfully, applied to H_3PO_3 adsorption isotherms obtained on bulk Pt [12]. In Equation (4), $\theta_{\mathrm{max},x(x=1,2)}$ is the maximum partial surface occupation of H_3PO_3 on crystalline plane *x*, *c* is the H_3PO_3 concentration in the electrolyte bulk and $K_{\mathrm{ads},x(x=1,2)}$ is the equilibrium adsorption constant of H_3PO_3 on crystalline plane *x*. All fitted parameters are included in the Supplementary Information (**Table S3**).

$$\theta = \frac{K_{\mathrm{ads},1}c}{K_{\mathrm{ads},1}c+1}\theta_{\mathrm{max},1} + \frac{K_{\mathrm{ads},2}c}{K_{\mathrm{ads},2}c+1}\theta_{\mathrm{max},2} \quad (4)$$

It must be noted that the shift and splitting of the CO oxidation peak observed at low H_3PO_3 concentrations (approximately 7×10^{-5} mol dm^{-3} H_3PO_3) is similar to that observed in the presence of non-purified H_3PO_4, providing a further strong indication that the species present in the non-purified acid is H_3PO_3.

Within this work, H_{upd} and CO stripping measurements were also performed on a polycrystalline Pt electrode. The purpose was to determine the effect of addition of H_3PO_4 to the 0.5 mol dm^{-3} $HClO_4$ solution, on the $ECSA_{Hupd}$ and $ECSA_{CO}$ values. It was shown that the effect of H_3PO_4, up to a concentration of 20 mmol dm^{-3}, on the both Pt ECSA values is only marginal. The determined $ECSA_{CO}$ values were on average 4 % higher than the $ECSA_H$ ones. Therefore, it seems that H_{upd} and CO stripping methods provide comparable values of ECSA on bulk Pt electrodes. Details are provided in section S7 in Supplementary information.

4. Conclusion

In the present work, the effect of H_3PO_4 purity on the behaviour of Pt/C thin film catalysts towards ORR was investigated and evaluated in diluted aqueous solutions at ambient conditions. Adding minute amounts of H_3PO_4 to the electrolyte in a model 3-electrode experimental set-up is a routine procedure to simulate the conditions and poisoning effects of a TF-RDE with Pt/C catalyst such as those expected to occur in the porous catalyst layer in a HT-PEMFC experiment. It was found that the impurity (most likely H_3PO_3) present in commercial 85 wt% H_3PO_4 (trace metal basis H_3PO_4) in the amount estimated to be about 0.07 mol.% blocks part of the ECSA and negatively influences ORR kinetics. This was most predominantly observed in the potential range below 0.75 V corresponding to the high current density region of the ORR. The same effect leads to a decrease in the limiting currents at electrode potentials as low as 0.5 V. At such low electrode potentials, H_3PO_3 is not oxidised at a measurable rate and accumulates at the Pt electrode surface instead. This accumulation was confirmed by the adsorption isotherms determined based on H_{upd}. The obtained adsorption isotherms revealed that the H_3PO_3 adsorption behaviour on Pt is not significantly affected by the presence of H_3PO_4 in concentrations of up to 0.1 mol dm^{-3}. It was also shown that CO stripping is very sensitive to the presence of H_3PO_3 even at low concentrations, which leads to an underestimation of ECSA due to the competition between H_3PO_3 and CO for Pt active sites. This causes changes in the CO oxidation peak position, height and width. In summary, H_3PO_3 seems to be the common impurity in otherwise highly pure commercial H_3PO_4 solutions. Its removal from H_3PO_4 is possible by treatment with H_2O_2 at elevated temperatures. This purification step seems to be essential for obtaining reproducible and reliable information about, e.g. ECSA, ORR and most likely also H_2 oxidation kinetics and mechanisms on Pt–based electrode surfaces. Similar results as with solutions prepared from purified H_3PO_4 were obtained with freshly dissolved solid (crystalline) H_3PO_4, which is, however, extremely costly.

CRediT authorship contribution statement

Bruna F. Gomes: Conceptualization, Methodology, Validation, Formal analysis, Investigation, Data curation, Writing – original draft, Visualization. **Martin Prokop:** Conceptualization, Methodology, Validation, Formal analysis, Investigation, Data curation, Writing – original draft, Visualization. **Tomas Bystron:** Conceptualization, Methodology, Formal analysis, Investigation, Data curation, Writing – original draft, Visualization. **Rameshwori Loukrakpam:** Methodology, Validation. **Carlos M.S. Lobo:** Writing – original draft. **Maximilian Kutter:** Methodology, Validation. **Timon E. Günther:** Methodology, Validation. **Michael Fink:** Methodology, Validation. **Karel Bouzek:** Conceptualization, Resources, Writing – original draft, Visualization, Supervision, Project administration, Funding acquisition. **Christina Roth:** Conceptualization, Methodology, Resources, Writing – original draft, Visualization, Supervision, Project administration, Funding acquisition.

Declaration of Competing Interest

The authors declare that they have no known competing financial interests or personal relationships that could have appeared to influence the work reported in this paper.

Acknowledgement

We gratefully acknowledge the DFG, German Research Foundation – Project-ID RO 2454/19-1, for the financial support. This study was supported by the Grant Agency of the Czech Republic under project No. 19-02964J. This study was supported by the European Regional Development Fund Project 'Fuel Cells with Low Platinum Content' (No. CZ.02.1.01/0.0/0.0/16_025/0007414).

Appendix A. Supplementary data

Supplementary data to this article can be found online at https://doi.org/10.1016/j.jelechem.2022.116450.

References

[1] J. Andrews, B. Shabani, Where does hydrogen fit in a sustainable energy economy?, Procedia Eng 49 (2012) 15–25.
[2] J. Andrews, B. Shabani, Re-envisioning the role of hydrogen in a sustainable energy economy, Int. J. Hydrogen Energy 37 (2) (2012) 1184–1203.
[3] S.S. Araya, F. Zhou, V. Liso, S.L. Sahlin, J.R. Vang, S. Thomas, X. Gao, C. Jeppesen, S.K. Kær, A comprehensive review of PBI-based high temperature PEM fuel cells, Int. J. Hydrogen Energy 41 (46) (2016) 21310–21344.
[4] R.E. Rosli, A.B. Sulong, W.R.W. Daud, M.A. Zulkifley, T. Husaini, M.I. Rosli, E.H. Majlan, M.A. Haque, A review of high-temperature proton exchange membrane fuel cell (HT-PEMFC) system, Int. J. Hydrogen Energy 42 (14) (2017) 9293–9314.
[5] R. Kerr, H.R. García, M. Rastedt, P. Wagner, S.M. Alfaro, M.T. Romero, C. Terkelsen, T. Steenberg, H.A. Hjuler, Lifetime and degradation of high temperature PEM membrane electrode assemblies, Int. J. Hydrogen Energy 40 (46) (2015) 16860–16866.
[6] M. Prokop et al, Degradation kinetics of Pt during high-temperature PEM fuel cell operation Part III: Voltage-dependent Pt degradation rate in single-cell experiments, Electrochim. Acta 363 (2020) 137165.
[7] Q. He, X. Yang, W. Chen, S. Mukerjee, B. Koel, S. Chen, Influence of phosphate anion adsorption on the kinetics of oxygen electroreduction on low index Pt(hkl) single crystals, PCCP 12 (39) (2010) 12544.
[8] K.-L. Hsueh, E.R. Gonzalez, S. Srinivasan, D.-T. Chin, Effects of phosphoric acid concentration on oxygen reduction kinetics at platinum, J. Electrochem. Soc. 131 (4) (1984) 823–828.
[9] S. Kaserer, K.M. Caldwell, D.E. Ramaker, C. Roth, Analyzing the influence of H3PO4 as catalyst poison in high temperature PEM fuel cells using in-operando X-ray absorption spectroscopy, J. Phys. Chem. C 117 (12) (2013) 6210–6217.
[10] F.C. Nart, T. Iwasita, On the adsorption of $H_2PO_4^-$ and H_3PO_4 on platinum: an in situ FT-ir study, Electrochim. Acta 37 (3) (1992) 385–391.
[11] N. Giordano, E. Passalacqua, P.L. Antonucci, L. Pino, M. Vivaldi, A. Patti, K. Kinoshita, Influence of physicochemical properties on the performance of Pt/C porous electrodes for oxygen reduction in phosphoric acid, Electrochim. Acta 38 (7) (1993) 913–918.
[12] M. Prokop, T. Bystron, M. Paidar, K. Bouzek, H3PO3 electrochemical behaviour on a bulk Pt electrode: adsorption and oxidation kinetics, Electrochim. Acta 212 (2016) 465–472.
[13] J.T. Glass, G.L. Cahen, G.E. Stoner, The Effect of Phosphoric Acid Concentration on Electrocatalysis, J. Electrochem. Soc. 136 (3) (1989) 656–660.
[14] N. Sugishima, J.T. Hinatsu, F.R. Foulkes, Phosphorous acid impurities in phosphoric acid fuel cell electrolytes II. Effects on the oxygen reduction reaction at platinum electrodes, J. Electrochem. Soc. 141 (12) (1994) 3332–3335.
[15] S.J. Clouser, J.C. Huang, E. Yeager, Temperature dependence of the Tafel slope for oxygen reduction on platinum in concentrated phosphoric acid, J. Appl. Electrochem. 23 (6) (1993) 597–605.
[16] S.B. Brummer, J.I. Ford, M.J. Turner, The adsorption and oxidation of hydrocarbons on noble metal electrodes. I. Propane adsorption on smooth platinum electrodes, J. Phys. Chem. 69 (10) (1965) 3424–3433.
[17] L. Trotochaud, S.L. Young, J.K. Ranney, S.W. Boettcher, Nickel-iron oxyhydroxide oxygen-evolution electrocatalysts: the role of intentional and incidental iron incorporation, J. Am. Chem. Soc. 136 (18) (2014) 6744–6753.
[18] M.C.O. Monteiro, M.T.M. Koper, Alumina contamination through polishing and its effect on hydrogen evolution on gold electrodes, Electrochim. Acta 325 (2019) 134915.
[19] K.J.J. Mayrhofer, A.S. Crampton, G.K.H. Wiberg, M. Arenz, Analysis of the impact of individual glass constituents on electrocatalysis on Pt electrodes in alkaline solution, J. Electrochem. Soc. 155 (6) (2008) P78.
[20] K.J.J. Mayrhofer, G.K.H. Wiberg, M. Arenz, Impact of glass corrosion on the electrocatalysis on Pt electrodes in alkaline electrolyte, J. Electrochem. Soc. 155 (1) (2008) P1.
[21] A. Tiwari, T. Maagaard, I.b. Chorkendorff, S. Horch, Effect of dissolved glassware on the structure-sensitive part of the Cu(111) voltammogram in KOH, ACS Energy Lett. 4 (7) (2019) 1645–1649.
[22] S. Trasatti, O.A. Petrii, Real surface area measurements in electrochemistry, J. Electroanal. Chem. 327 (1) (1992) 353–376.
[23] D.F. van der Vliet, C. Wang, D. Li, A.P. Paulikas, J. Greeley, R.B. Rankin, D. Strmcnik, D. Tripkovic, N.M. Markovic, V.R. Stamenkovic, Unique electrochemical adsorption properties of Pt-skin surfaces, Angew. Chem. Int. Ed. 51 (13) (2012) 3139–3142.
[24] M. Inaba, A.W. Jensen, G.W. Sievers, M. Escudero-Escribano, A. Zana, M. Arenz, Benchmarking high surface area electrocatalysts in a gas diffusion electrode: measurement of oxygen reduction activities under realistic conditions, Energy Environ. Sci. 11 (4) (2018) 988–994.
[25] K.J.J. Mayrhofer, D. Strmcnik, B.B. Blizanac, V. Stamenkovic, M. Arenz, N.M. Markovic, Measurement of oxygen reduction activities via the rotating disc electrode method: From Pt model surfaces to carbon-supported high surface area catalysts, Electrochim. Acta 53 (7) (2008) 3181–3188.
[26] S. Rudi, C. Cui, L. Gan, P. Strasser, Comparative study of the electrocatalytically active surface areas (ECSAs) of Pt alloy nanoparticles evaluated by Hupd and CO-stripping voltammetry, Electrocatalysis 5 (4) (2014) 408–418.
[27] M. Prokop, T. Bystron, K. Bouzek, Electrochemistry of phosphorous and hypophosphorous acid on a pt electrode, Electrochim. Acta 160 (2015) 214–218.
[28] Y. Garsany, I.L. Singer, K.E. Swider-Lyons, Impact of film drying procedures on RDE characterization of Pt/VC electrocatalysts, J. Electroanal. Chem. 662 (2) (2011) 396–406.
[29] P.N.J. Ross, P.C. Andricacos, The effect of H2POV anion on the kinetics of oxygen reduction on Pt, J. Electroanal. Chem. 154 (1983) 205–215.
[30] M.J.S. Farias, G.A. Camara, J.M. Feliu, Understanding the CO preoxidation and the intrinsic catalytic activity of step sites in stepped Pt surfaces in acidic medium, The Journal of Physical Chemistry C 119 (35) (2015) 20272–20282.
[31] M.J.S. Farias, W. Cheuquepán, A.A. Tanaka, J.M. Feliu, Requirement of initial long-range substrate structure in unusual CO pre-oxidation on Pt(111) electrodes, Electrochem. Commun. 97 (2018) 60–63.
[32] P.P. Lopes, D. Tripkovic, P.F.B.D. Martins, D. Strmcnik, E.A. Ticianelli, V.R. Stamenkovic, N.M. Markovic, Dynamics of electrochemical Pt dissolution at atomic and molecular levels, J. Electroanal. Chem. 819 (2018) 123–129.
[33] P. Daubinger, J. Kieninger, T. Unmüssig, G.A. Urban, Electrochemical characteristics of nanostructured platinum electrodes – a cyclic voltammetry study, PCCP 16 (18) (2014) 8392–8399.
[34] A. Damjanovic, V. Brusic, Electrode kinetics of oxygen reduction on oxide-free platinum electrodes, Electrochim. Acta 12 (6) (1967) 615–628.
[35] A. Holewinski, S. Linic, Elementary mechanisms in electrocatalysis: revisiting the ORR tafel slope, J. Electrochem. Soc. 159 (11) (2012) H864–H870.
[36] C. Wang, Y.-B. Zhong, J. Wang, Z.-Q. Wang, W.-L. Ren, Z.-S. Lei, Z.-M. Ren, Effect of magnetic field on electroplating Ni/nano-Al2O3 composite coating, J. Electroanal. Chem. 630 (1-2) (2009) 42–48.
[37] K. Shinozaki et al, Oxygen reduction reaction measurements on platinum electrocatalysts utilizing rotating disk electrode technique, J. Electrochem. Soc. 162 (12) (2015) F1384–F1396.
[38] H. Yang, S. Kumar, S. Zou, Electroreduction of O_2 on uniform arrays of Pt nanoparticles, J. Electroanal. Chem. 688 (2013) 180–188.
[39] J. Huang, X. Zhu, M. Eikerling, The rate-determining term of electrocatalytic reactions with first-order kinetics, Electrochim. Acta 393 (2021) 139019.
[40] J. Huang, J. Zhang, M. Eikerling, Unifying theoretical framework for deciphering the oxygen reduction reaction on platinum, PCCP 20 (17) (2018) 11776–11786.
[41] A. Parthasarathy, S. Srinivasan, A.J. Appleby, C.R. Martin, Temperature dependence of the electrode kinetics of oxygen reduction at the platinum/Nafion® interface—A microelectrode investigation, J. Electrochem. Soc. 139 (9) (1992) 2530–2537.

[42] R. Halseid, T. Bystroň, R. Tunold, Oxygen reduction on platinum in aqueous sulphuric acid in the presence of ammonium, Electrochim. Acta 51 (13) (2006) 2737–2742.
[43] J.X. Wang, J. Zhang, R.R. Adzic, Double-trap kinetic equation for the oxygen reduction reaction on Pt(111) in acidic media, J. Phys. Chem. A 111 (49) (2007) 12702–12710.
[44] T. Shinagawa, A.T. Garcia-Esparza, K. Takanabe, Insight on Tafel slopes from a microkinetic analysis of aqueous electrocatalysis for energy conversion, Sci. Rep. 5 (1) (2015) 13801.
[45] S. Weisenberger, A. Schumpe, Estimation of gas solubilities in salt solutions at temperatures from 273 K to 363 K, AIChE J. 42 (1) (1996) 298–300.